ISSN 1674-1056
http://cpb.iphy.ac.cn
http://iopscience.iop.org/cpb
中国物理 B
Chinese Physics
中国物理 Chinese Physics B

Comparisons of electrical and optical properties between graphene and silicene-A review

Wirth-Lima A J, Silva M G, Sombra A S B
Citation: Chin. Phys. B . 2018, 27(2): 023201. **doi:** 10.1088/1674-1056/27/2/023201

Journal homepage: http://cpb.iphy.ac.cn; http://iopscience.iop.org/cpb

What follows is a list of articles you may be interested in

Numerical study on discharge characteristics influenced by secondary electron emission in capacitive RF argon glow discharges by fluid modeling

Lu-Lu Zhao(赵璐璐), Yue Liu(刘悦), Tagra Samir
Chin. Phys. B . 2018, 27(2): 025201. **doi:** 10.1088/1674-1056/27/2/025201

Numerical study on the gas heating mechanism in pulse-modulated radio-frequency glow discharge

Qi Wang(王奇), Xiao-Li Yu(于晓丽), De-Zhen Wang(王德真)
Chin. Phys. B . 2017, 26(3): 035201. **doi:** 10.1088/1674-1056/26/3/035201

Study of hysteresis behavior in reactive sputtering of cylindrical magnetron plasma

H. Kakati, S. M. Borah
Chin. Phys. B . 2015, 24(12): 125201. **doi:** 10.1088/1674-1056/24/12/125201

Field ionization process of Eu $4f^7 6snp$ Rydberg states

Zhang Jing, Shen Li, Dai Chang-Jian
Chin. Phys. B . 2015, 24(11): 0113201. **doi:** 10.1088/1674-1056/24/11/113201

Precision frequency measurement of $^1S_0$-$^3P_1$ intercombination lines of Sr isotopes

Liu Hui, Gao Feng, Wang Ye-Bing, Tian Xiao, Ren Jie, Lu Ben-Quan, Xu Qin-Fang, Xie Yu-Lin, Chang Hong
Chin. Phys. B . 2015, 24(1): 013201. **doi:** 10.1088/1674-1056/24/1/013201

Comparisons of electrical and optical properties between graphene and silicene — A review*

Wirth-Lima A J[1,2,†], Silva M G[3], and Sombra A S B[1,2]

[1] Laboratory of Telecommunications and Materials Science and Engineering-www.locem.ufc.br - Fortaleza, Ceará, Brazil
[2] Department of Physics, Science Center, Federal University of Ceará (U.F.C.) - Fortaleza, Ceará, Brazil
[3] State University of Vale do Acaraú, Sobral, Ceará, Brasil

(Received 26 August 2017; revised manuscript received 18 October 2017; published online 5 January 2018)

Two-dimensional (2D) metamaterials are considered to be of enormous relevance to the progress of all exact sciences. Since the discovery of graphene, researchers have increasingly investigated in depth the details of electrical/optical properties pertinent to other 2D metamaterials, including those relating to the silicene. In this review are included the details and comparisons of the atomic structures, energy diagram bands, substrates, charge densities, charge mobilities, conductivities, absorptions, electrical permittivities, dispersion relations of the wave vectors, and supported electromagnetic modes related to graphene and silicene. Hence, this review can help readers to acquire, recover or increase the necessary technological basis for the development of more specific studies on graphene and silicene.

Keywords: graphene, silicene, electrical/optical properties

PACS: 32.30.Jc, 52.20.–j, 52.25.Dg, 52.25.Fi **DOI:** 10.1088/1674-1056/27/2/023201

1. Introduction

German chemists Ulrich Hofmann and Hanns-Peter Boehm studied the two-dimensional (2D) planar structure of carbon atoms, which Boehm called graphene (1962). However, the properties of this material had been unknown for decades until it fascinatingly reappeared in 2004 at the University of Manchester, where Dutchman Geim (director of the physics department of that university), and Novoselov (postdoctoral researcher) studied the creation of a substance obtained from graphite. In their experiments they sought to obtain the thinnest possible slice from graphite, in order to study the behavior of this new material. Fortunately, those scientists observed the graphene predicted in 1962 in the fragments stuck in a tape used to clean the surface of a block of graphite. Then, these residues were examined in an atomic microscope and they observed that this new material (graphene) could function as a transistor. After this new discovery on the physical characteristics of graphene, the team of Geim and Novoselov made that material thinner and thinner, until it reached a thickness of an atom. On the other hand, they also found that this ultrafine material not only maintained a hexagonal bonding structure, but also had a peculiar symmetrical arrangement of electrons, which provided an increase in its conductivity. The discovery of the properties of graphene was published by Geim and Novoselov in 2004, which gave these two scientists the Nobel Prize in Physics six years later. Since then, research on graphene has begun in various parts of the world.

Currently, researchers around the world are increasingly going deeper into the detailing of electrical/optical properties related to other 2D metamaterials, especially silicene, which is named 2D silicon. The term silicene was introduced by Gusmán–Verry and Lew Yan Voon in 2007.

The huge interest in silicene occurs due to the preservation of the use of silicon in the optoelectronics industry. Note that the constant advance in the technology related to silicene allows us to infer that it will probably be possible to find the solution to enable Moore's law in dimensions smaller than 10 nm. Another reason for the development of silicene-based technology is that while silicene is the second largest element in the Earth's crust (28.2%), the carbon (from which graphene is obtained) is only 0.02%.

2. Atomic structures

The carbon atoms in 2D graphene (contained in a plane) form a honeycomb lattice consisting of carbon atoms with sp^2 hybrid covalent bonds. However, this honeycomb lattice is not of a conventional Bravais structure, since the atomic structures referring to two of the adjacent atoms are not equivalent.[1]

Figure 1(a) shows the honeycomb atomic structure of grapheme, graphene, and figure 1(b) shows a hexagonal atomic structure of Bravais (conventional). Note that the honeycomb structure lacks an atom located in the central part of the hexagon, so that this atomic structure cannot be considered as a hexagonal atomic structure, which is a conventional Bravais structure. It is worth noting that an atomic structure can only be considered a Bravais structure when all the points

*Project supported by the National Council for Scientific and Technological Development (CNPq).
†Corresponding author. E-mail: awljeng@gmail.com
© 2018 Chinese Physical Society and IOP Publishing Ltd

of this network are equivalent, so that the connection between any two points of the atomic structure can be obtained through the unit vectors of this network.

In the honeycomb atomic structure of graphene, its unit cell can be defined as a rhombus, where two carbon atoms are located, according to what is shown in Fig. 1(a).

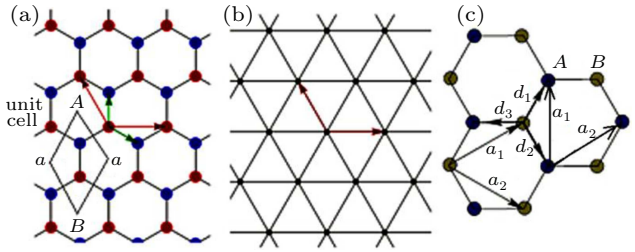


Fig. 1. (color online) (a) Unit cell related to the atomic structure of graphene (rhombus). (b) Hexagonal atomic structure. (c) Unit vectors referring to the atomic structure of graphene (a_1 and a_2).

As we can see in Fig. 1(c), the two atoms (A and B) of the unit cell constitute two non-equivalent atoms because these two atoms cannot be connected with one or with a combination of the unit vectors a_1 and a_2.

Since the honeycomb atomic structure of graphene can be considered as an association of two triangular atomic structures, forming a Bravais structure, in the honeycomb structure of graphene, the vectors a_1 and a_2 are the unit vectors, and d_1, d_2, and d_3 (Fig. 1(c)) are the vectors that determine the closest distances (between neighboring atoms). This distance between adjacent carbon atoms (a_0) has a value equal to 0.142 nm, which is the average distance between the covalent (C–C) and double (C=C) covalent bonds that make up a graphene layer. Given that the lengths of the unit vectors are all given by $a = \sqrt{3}a_0$, these unit vectors have length $a = 0.246$ nm, so that

$$a_1 = \left(\frac{\sqrt{3}a_0}{2}, \frac{a_0}{2}\right); \quad a_2 = \left(\frac{\sqrt{3}a_0}{2}, -\frac{a_0}{2}\right). \tag{1}$$

Note that the three points closest to a given point in the direct graphene structure are given by

$$d_1 = \frac{a_0}{2}\left(1, \sqrt{3}\right); \quad d_1 = \frac{a_0}{2}\left(1, -\sqrt{3}\right); \quad d_3 = a_0(1,0), \tag{2}$$

and the six points with the second closest proximity are given by

$$d'_1 = \pm a_1; \quad d'_2 = \pm a_2; \quad d'_3 = \pm(a_2 - a_1). \tag{3}$$

The first Brillouin zone of the graphene is presented in Fig. 2, in which the unit vectors are also shown to be ($|b_1| = |b_2| = 4\pi/\sqrt{3}a$) where

$$b_1 = \left(\frac{2\pi}{\sqrt{3}a}\frac{2\pi}{3a}\right); \quad b_2 = \frac{2\pi}{3a_0}\left(\frac{2\pi}{\sqrt{3}a}, -\frac{2\pi}{3a}\right). \tag{4}$$

The points K and K' shown in Fig. 2 are called Dirac points, which are very important for detailing the electrical properties of graphene, according to what will be seen later. The locations of these points in the k space are given by

$$K = \left(\frac{2\pi}{\sqrt{3}a}, \frac{2\pi}{3a}\right); \quad K' = \left(\frac{2\pi}{\sqrt{3}a}, -\frac{2\pi}{3a}\right). \tag{5}$$

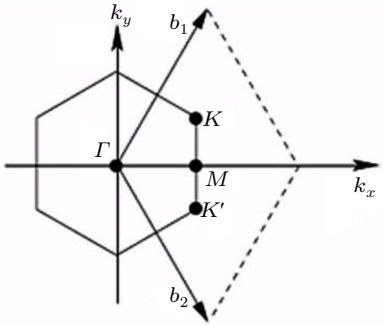


Fig. 2. Reciprocal structure and first Brillouin zone of graphene.

On the other hand, the silicene is constituted by a layer of atoms also forming a honeycomb atomic structure, which is obtained from the three-dimensional (3D) silicon and has sp^3 hybrid covalent bonds. The electrical and optical properties of silicene can be obtained from the density-functional theory (DFT). It has been proven that in the atomic structure of the silicene, B atoms of a unit cell identical to that of the graphene would need to be slightly displaced with respect to the A atoms of that unit cell. That buckled structure (Fig. 3(a)) makes sense, since it is very similar to the plane (111) of the 3D silicon.[2] It is noteworthy that although the carbon and silicon atoms are in the same column (group 14 of the periodic table), the carbon is located in line 2 and the silicon in line 3 of this periodic table, so that these elements have different chemical properties. For example, the energy difference between the valence orbitals for the s and p orbitals has a value of 10.66 eV for carbon and it has a value of 5.66 eV for silicon.[3] Therefore, in the silicon atom the preference is the use of the three p orbitals, resulting in sp^3 hybridizations.

Due to the significant increase in the silicene atomic distance in relation to the graphene, the π–π overlap in silicene decreases by roughly an order of magnitude, so that the Si=Si bonds are, in general, much weaker than C=C bonds. That is the reason why silicene has a buckled atomic structure and does not exist naturally, unlike graphene, which has a flat atomic structure.

As the bonds between silicon atoms in the silicene are a mixture of sp^2 and sp^3 hybridizations, we can state that there is no natural silicene, which means that the silicene cannot be obtained via exfoliation.[4]

It is worth mentioning that the angle between the π bonds (perpendicular to the plane) and the σ bonds (in the plane) referring to the sp^2 hybrids in the graphene has a value of 90°. However, due to sp^3 hybridizations in 3D silicon, the angle between the bonds is higher (109.47°) and in the buckled plane of the silicene, where a mixture between the sp^2 and

sp^3 hybridizations occurs, the angle between the bond normal to the plane and the bonds in the buckled plane has a value of 101.73°.[5]

The distance between neighboring silicon atoms (a_0) has a value approximately equal to 0.2217 nm. As we can see from Fig. 3(a), the unit cell of silicene, just as in graphene, consists of two atoms (A and B), but the unit cell of the silicene has a structure parameter $a \approx 0.384$ nm. Therefore, the atomic structure of the silicene has the same properties as those presented above with respect to the graphene, except that in the silicene there is a vertical displacement between the atoms A and B ($\delta = 0.045$ nm) as shown in Fig. 3(b). It is noteworthy that in the 3D silicon the displacement of the atoms relative to the plane (1,1,1) is 0,078 nm.[6–8]

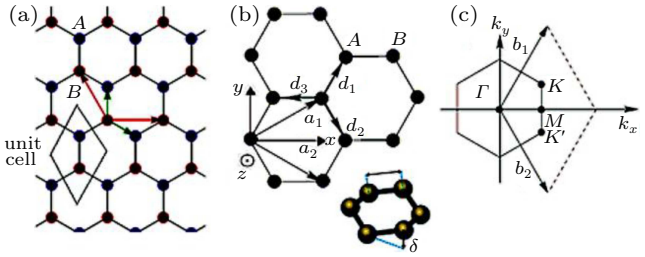


Fig. 3. (color online) Atomic structure and first Brillouin zone of silicene.

We can see from Fig. 3(c) that the first Brillouin zone for the reciprocal structure of the silicene has the same shape as the first Brillouin zone for the reciprocal structure of the graphene. Note that the locations of the K points are given according to Eq. (5), by changing only the value of the structure parameter.

The bonding energy between the silicon atoms in the silicene is 4.9 eV/atom, while in the 3D silicon (diamond-like structure) it is 0.6 eV/atom.[7]

Presently, the manner of obtaining silicene is by synthesizing on a substrate. Some methods have already been presented, in order to obtain the synthesis of epitaxial layers of silicene on substrates of silver (111),[9–14] iridium (111),[14] and zirconium diboride.[15] (It is obvious that the epitaxial growth consists of obtaining thin layers on crystalline substrates. We will come back to this subject further).

Possible occurrence of superconductivity in silicene on silver (111) at 35 K–40 K was also observed, which is the highest among those temperatures observed in superconducting elements.[16,17]

A buckled structure of silicon atoms has also been investigated and defined as Si (111), since it can be seen as a plane of Si (111).[18]

3. Energy band diagrams

It is already well known that graphene has zero band gap, which makes it difficult to use in field effect transistors. On the other hand, silicene can behave as a semimetal with a band gap that is variable, by the application of an external electric field, or as a metal.[19–22]

Like the case of graphene, the energy bands π and π^* of the silicene energy dispersion relation touch the Dirac K point and have a linear relationship in the vicinity of that point. That dispersion relations of graphene and silicene can be calculated by means of the DFT[23] as shown in Fig. 4.

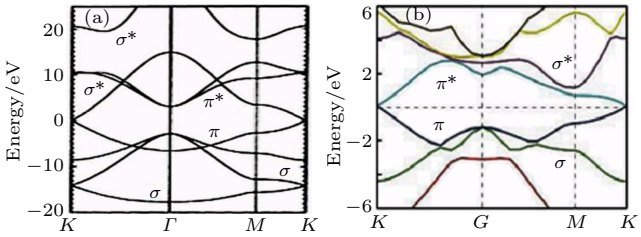


Fig. 4. (color online) (a) Energy band structure of graphene. (b) Energy band structure of silicene.

Graphene and silicene are referred to as "intrinsic" (without doping), when the Fermi energy (whose value is approximately equal to the chemical potential) at Dirac points has zero value. Indeed, we can hardly find, for example, intrinsic graphene, since small spatial heterogeneities always occur. On the other hand, these two 2D metamaterials (graphene and silicene) are called "extrinsic" (doped), when electrons are introduced into the conduction band (or holes in the valence band), such as through gate voltage, according to what we will see more ahead.

In intrinsic graphene and silicene, for low energy levels around the Dirac point (K), the dispersion relation is linear and can be expressed mathematically through $E(q) = \pm V_F \hbar |q|$, where the symbol $+$ represents the conduction band and the symbol $-$ refers to the valence band, $q = k - K = \sqrt{q_x^2 + q_y^2}$ is the wave vector with respect to the Dirac point and $V_F = 10^6$ m/s is Fermi velocity on graphene. This linear relation is valid until energy values related to the visible light, so that the frequencies used in telecommunication are also included. Therefore, graphene and silicene in their original states (without doping) have Fermi energy $E_F = 0$ at K points of the Brillouin zone (Dirac points), where the valence band is completely filled, while the conduction band is completely empty, and the conduction and valence bands touch the K points. Although this property is very useful in many applications, it is an obstacle to the use of graphene in nanoelectronic devices, such as FETs, for example. This is because it is very difficult to open a band gap in the graphene dispersion relation, while preserving its electronic properties, given that its atomic structure is completely contained in a plane.

On the other hand, due to the fact that the electronic structure of the silicene is buckled with respect to the plane, it is possible to open a band gap in the dispersion relation of the silicene, with the preservation of its electronic properties. This is due to the interactions between silicene and substrate

atomic structures, which provide a difference in energy between the electrons located in these two superstructures (Δ). Consequently, the band gap caused at the Dirac point (K) is given by $E_{gs} = 2\Delta$. Considering that in this case the Van der Waals interactions are weak, the value of Δ is small, which implies a small value for the band gap. It is worth mentioning that the value of this band gap can be increased by changing the interaction between the two substrates, or by means of the gate voltage.

In the case of the application of a gate voltage, the open energy range (E_g) increases linearly with the increase in the value of the perpendicular applied electric field ($E_\perp$), according to what can be demonstrated by the density theory (DFT). This occurs due to the fact that this applied electric field causes the symmetry to break between the substructures of the silicene (A and B), which causes a band gap to be opened. The total band gap value is the sum of $E_g + E_{gs}$. However, taking into account that the E_{gs} value for silicene on h-BN (substrate used will be presented below) is very small, we neglect E_{gs}.

Note that the band gap ($E_g = eE_\perp \delta$, where e is the charge of the electron and $\delta \approx 0.044$ nm is the vertical displacement between the silicene atomic substructures) increases linearly with the increase of $E_\perp$.[23]

Considering the operation of an electric field perpendicular to the plane of the silicene, we can represent the band structure in the vicinity of the K point for the device shown in Fig. 5, according to the following equation:[24]

$$E = \pm\sqrt{E_g^2 + (\hbar V_F q)^2}, \tag{6}$$

where $\hbar$ is the reduced Planck constant, $V_F = 1.3 \times 10^6$ m/s is the Fermi velocity in silicene and $q = \sqrt{q_x^2 + q_y^2}$ is the wave number around K.

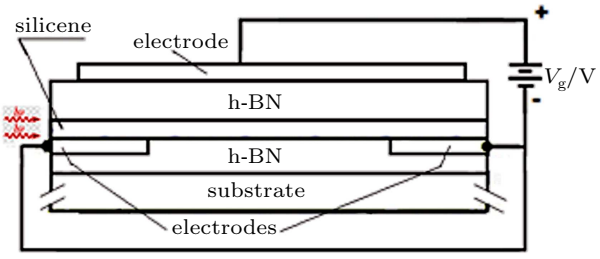


Fig. 5. (color online) Schematic representation of a silicene-based field effect transistor.

Since the device shown above is a waveguide (which can be controlled via gate voltage), the photons incident on the nanoribbon are coupled to the surface plasmons (SPs) modes, forming what is called surface plasmons polaritons (SPPs).

Recent experiments were carried out with the objective of investigating the process of coupling of radiation emitted by a transmitter located above to the plane of a graphene ribbon (distance $d = 50$ nm) and to the side, i.e., in the same plane (distance $d = 50$ nm) of a graphene ribbon. It is noteworthy that the emitted radiation coupled with the plasmons on the surface of graphene forming GSPPs.[25] In these experiments, the emitter was considered as an electric dipole and the thickness of graphene was assumed to be 0.5 nm. The coupling efficiency was defined as the ratio between the decay rate of total energy emitted by the optical source and the decay rate of energy emitted by the optical source that is transformed in GSPPs, that is, the greater the coupling efficiency, the greater the amount of energy coming from the optical source that is transformed into GSPPs, so that the smaller the dissipation loss is. It was verified (theoretically and numerically) that the coupling efficiencies in the two cases both depend on the polarization direction of the emitted light and that the decay rate of the optical source to form GSPPs when the emitting optical source is located in the same plane of the graphene is 10 times greater than that when this source is located above the graphene plane.[25]

The width of the nanoribbon strongly influences the behaviors of the propagating modes. Briefly, the smaller the width of the nanoribbon (W), the smaller the number of modes present in the waveguide. Previous studies have revealed that in a graphene nanoribbon with width less than 50 nm, there is a single propagating mode (fundamental mode).[26] However, when $W < 10$ nm, finite-size effects become important, so that the classical theory of local electromagnetism can no longer determine the behavior of GSPPs.[27]

In fact, unlike what occurs in conventional waveguides, where the waveguide width is given by $\lambda/2$, the GSPP modes that can propagate in a homogeneous graphene nanoribbon with a given width are determined by quite a different mathematical formulation based among other parameters, on the width of the nanowire.[26] We adopted the width of the nanoribbon $W = 25$ nm.

We can find the length of the nanoribbon as a function of the propagation length in which a GSPP mode undergoes energy decay in the form of $(1 - 1/e)$ from its initial energy. However, there are other factors that influence the length calculation, such as dispersions and non-linear effects. We adopted the length of the nanowire $L = 250$ nm.[28]

Taking into account that we will present the detailing referring to the opening of a band gap for a layer of silicene, we use a layer of silicene in the device shown in Fig. 5.

The thickness of the h-BN layer was adopted as $d = 12$ nm, according to what will be detailed below. The h-BN layer located below the silicene layer is supported by an SiO_2 substrate with a thickness of 300 nm, which in turn is supported by a silicon substrate.

Considering the dielectric constant of h-BN $\varepsilon_d \approx 3.4$,[29] we can conclude by Eq. (6) that the larger the value of E_g, the greater the gap value at the Dirac point (K), as shown in the

following Fig. 6.

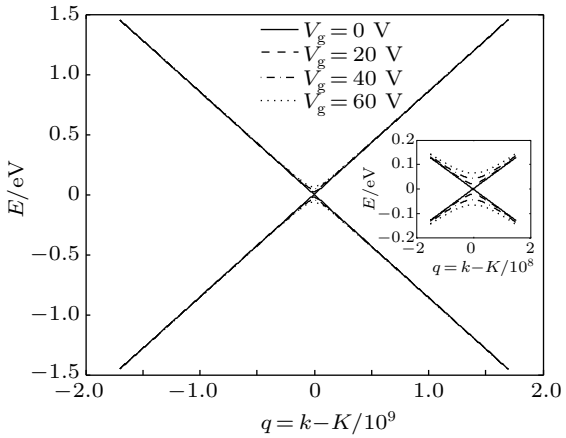


Fig. 6. Energy versus wave vector near the K point.

Graphene nanoribbons can tolerate electric current density greater than 10^8 A/cm^2, for widths less than 16 nm. This breaking current density has a reciprocal relationship to the resistivity of graphene nanofite. Joule heating is the most likely mechanism of breaking.[30]

On the other hand, the atomic structure of the silicene is preserved until $E_\perp = 2.6$ V/Å.[31]

Figure 6 shows the variations of energy (in unit eV) of the modes present in the silicene nanoribbon with wave number.

The range of values of wave numbers was selected in order to allow propagation of SPP modes up to the frequency range used in optical telecommunications. Note the existence of the gaps, according to what was mentioned above.

It is worth noting that in the absence of the electric field, the dispersion relations of silicene and graphene are similar ($E = \hbar V_F |q|$), with small deviations in the values, due to the fact that the Fermi velocity in the silicene is slightly higher than in the graphene, according to what was mentioned previously.

4. Substrates

A graphene nanoribbon has roughness due to several factors. Then, the substrate on which the graphene nanoribbon is supported must conform to the roughness, i.e., graphene after transferring, must be free of wrinkles or distortions. Thermal deposition of SiO_2 generally results in high surface roughness. In addition, graphene on SiO_2 does not show charge homogeneity along its surface.

On the other hand, hexagonal boron nitride (h-BN), termed white graphite, is also contained in a plane. This material is an isomorphic graphite, in which the boron and nitrogen atoms are located at points A and B of the graphene atomic structure. Therefore, the atomic structure of h-BN is similar to the atomic structure of graphene. The space between two layers of graphite is 0.355 nm and the space between two layers of h-BN is 0.333 nm.[32]

Since the roughness of the surface of the h-BN layer is much smaller than the roughness of the SiO_2 surface, the graphene nanoribbon is much better positioned on the surface of h-BN.

There are several methods of depositing f h-BN layers on the SiO_2/Si. However, despite the similarity between those two materials, graphene can be considered as a semiconductor with zero bandgap, while h-BN is considered as an insulator, whose bandgap has a value equal to 5.9 eV.[33]

Graphene and h-BN have very strong covalent bonds in the plane, and weak Van der Waals bonds between adjacent planes. However, the atomic bonds in the h-BN are approximately ionic, when compared with the atomic bonds of the graphene.[34]

Considering the fact that the roughness of h-BN is much smaller than the roughness of SiO_2, graphene embedded between layers of h-BN has charge mobility and charge homogeinity with values that are almost an order of magnitude higher than those embedded between layers of SiO_2. From the Drude formula it was determined that the charge mobility for graphene supported by h-BN varies from 2.5×10^4 cm^2/V·s at high charge density(in agreement with the Hall mobility) to 1.4×10^5 cm^2/V·s near the charge neutrality point.[35] Hence, we determine the value of the charge mobility on graphene over h-BN to be $\mu = 2.5 \times 10^4$ cm^2/V·s at high charge densities.

The graphene (or silicene) layer in our device is embedded between two layers of h-BN, the h-BN layer being located below the graphene (or silicene) and it is supported on a substrate consisting of SiO_2, which in turn is supported on a silicon substrate. The thickness of the h-BN layer located above the graphene (or silicene) layer should be $\approx>$ 10 nm in order to smooth the roughness of the SiO_2 layer, as well as to prevent the graphene layer from receiving unwanted charge carriers. On the other hand, the thickness of this layer of h-BN must be $\approx<$ 70 nm, to assure the operation of the gate voltage applied to the graphene (or to the silicene).

Mechanical exfoliation method of making graphene, which is actually contained in a plane, does not work for silicene. So far, the main method of synthesizing silicene is by means of epitaxial growth.

In the initial method of obtaining a small amount of silicon sheet, silver substrates Ag (001)[36] and Ag (110)[37] were used. After this, several experiments were elaborated with the objective of producing the silicene by means of epitaxial growth on Ag (111) surfaces. Since the atomic structure of the silicene is buckled, this atomic structure becomes changed due to the interaction with the atomic structure of the substrate. Hence, several superstructures referring to the silicene were observed during these experiments. Examples of these superstructures are (4×4), $\sqrt{13} \times \sqrt{13})$ R13.9°, $\sqrt{7} \times \sqrt{7})$ R19.1°, $2\sqrt{3} \times 2\sqrt{3})$ R30° (with respect to the atomic structure of

Ag (111)[38–40] and $\sqrt{3}\times\sqrt{3}$) (relative to the structure of the silicene (1×1)).[38,41,42] The reason forchoosing silver as a substrate for the growth of the silicene is due to the fact that this material provides a moderate and homogeneous interaction with the silicene, which results in very moderate tensions in the silicene in the process of growth.[43]

In the superstructure (4×4), the silicene sheet is positioned on the surface of Ag (111), so that a supercell (3×3) of the silicene coincides with a supercell (4×4) of Ag (111).

The superstructure (4×4) is called "magic incompatibility", which is due to the fact that we can consider the silver structure parameter (is) as $a_{\mathrm{Ag}}=0.288$ nm and the silicene structure parameter (is) as $a_{\mathrm{Si}}=0.384$ nm, which gives the ratio $4\times a_{\mathrm{Ag}}=3\times a_{\mathrm{Si}}$. Note that the two atomic structures (Ag (111) and silicene) are hexagonal. Consequently, the interference between the two superstructures is minimal, which provides the stabilization of the atomic structure of the silicene, according to what is shown in Fig. 7.[44,45]

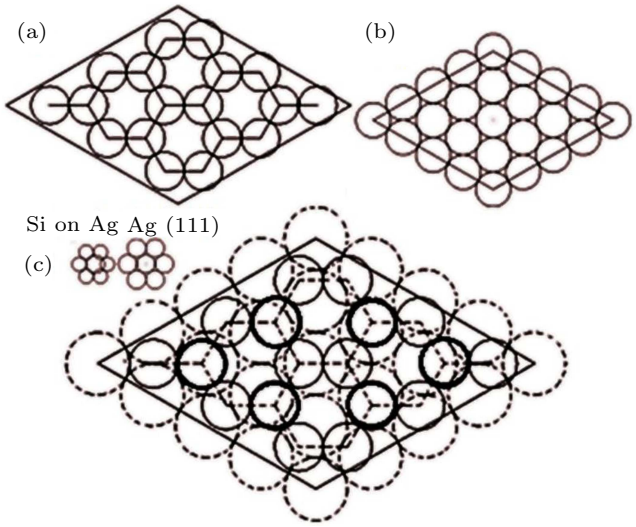


Fig. 7. (a) Schematic representation referring to the 3×3 superstructure of the isolated silicene. (b) Schematic representation of the 4×4 superstructure of the Ag (111) surface. (c) Schematic representation of the superstructure $(4\times4)-\alpha$.

The 4×4 superstructure can be obtained by placing a silicene (1×1) structure on the Ag (111)-1×1 structure. However, since the silicene atomic structure does not completely coincide with the atomic structure of silver (111), the silicene atoms are located between, or above, the Ag atoms (Fig. 7).

We can state that from the structure parameter of the silicon unit cell ($a\approx0.384$ nm), it is easy to find the distance between neighboring silicon atoms (≈0.2217 nm). Note that the covalent radius is ≈0.11085 nm. Recall that in 3D silicon the atomic radius is 0.118 nm. On the other hand, the atomic radius of the silver atom is $r_{\mathrm{Ag}}=0.144$ nm and the silver (111) structure parameter is $a_{\mathrm{Ag}}=0.288$ nm.

The 3×3 superstructure of the silicene is shown in Fig. 7(a), and the 4×4 superstructure related to Ag (111) is shown in Fig. 7(b). Figure 7(c) represents the overlap of the 3×3 superstructure of the silicene on the 4×4 superstructure of Ag (111).

Since the covalent radius of the silicon atom in the silicene (solid lines) is smaller than the atomic radius of the silver atom (dash lines), it is not possible to place silicon atoms forming a hexagon, tangent to the silver atoms in accordance with what can be observed in the detail inserted in Fig. 7(c).

The scanning tunneling microscope (STM) image shows that in the Si (3×3) superstructure on Ag (4×4) superstructure there are six protrusions in each unit (due to the higher atoms of the silicene), which does not happen in the Moiré pattern. Given that in the 3×3 superstructure of silicene there are 18 silicon atoms, half of these atoms would be at the highest level and the other half at the lower level. However, when the silicene is placed on the surface of the substrate constituted by Ag (111), the buckled structure of silicene causes the energy surface to lower. Then, due to this energy reorganization, there are only 6 silicene atoms at the highest positions and 12 silicene atoms at the lower positions of the Si (3×3) superstructure[40,46] as shown in Fig. 7(c).[44]

Note that three of the six silicene atoms located at the upper level of this 3×3 superstructure belong to one half of the superstructure and the other three silicene atoms belong to the other half of that superstructure. The highlighted circles in Fig. 7(c) represent the atoms located at the highest level.

The configuration of this Si (3×3) superstructure on Ag (4×4) superstructure is called a 4×4–α phase.[40] In the 4×4–α phase, the six higher atoms do not belong to the same atomic substructure of the silicene (it is unlikely to happen in the isolated silicene, in which all the higher silicon atoms belong to the same atomic substructure and all the lower atoms belong to the other atomic substructure). Furthermore, the 4×4–α phase is not located on the edges of the silicene sheet. On these edges there is another configuration called a 4×4–β phase. The configurations of these two phases are different, probably due to the fact that the phase $(4\times4$–$\beta)$ is less stable than the other phase $(4\times4$–$\alpha)$, but the stresses that emerge at the ends of the silicene sheet help stabilize the silicene atoms.[46] In addition to the Si (3×3) superstructure on Ag (4×4) superstructure detailed above, there are four other configurations (phases) of possible superstructures relating to the silicene on Ag (111), depending on the temperature to which the substrate is subjected.

For temperatures below 400 K, the silicon atoms deposited on the surface of Ag (111) tend to form disordered atomic structures.[47] However, for temperatures above 400 K during the deposition of the silicon atoms, the obtained silicene sheet exhibits the superstructure phases 4×4, $\sqrt{13}\times\sqrt{13}$ R13.9°, $\sqrt{7}\times\sqrt{7}$ R19.1°, $2\sqrt{3}\times2\sqrt{3}$ R30°, and $\sqrt{3}\times\sqrt{3}$, depending on the increase of the substrate temperature.

Other processes for obtaining silicene have appeared since 2012, such as the synthesis on various substrates by the

direct deposition of silicon atoms and annealing at 670 K, including the surfaces of Ag (111), zirconium diboride–ZrB_2 (0001),[15] and iridium Ir (111).[48]

A highly wrinkled sheet of silicene was fabricated on a molybdenum disulfide (MoS_2) semiconductor substrate, which represents the possibility of obtaining an isolated sheet of silicene, thus avoiding the influence of the metal substrate on the electronic structure of the silicene.[49]

In addition, multilayer silicene sheets were manufactured on Ag (111) surfaces by using epitaxial technology.[39,50–55]

Since the surface of the silicene is chemically active, chemical adsorbents can be used, which can change the electrical/optical properties of the silicene, such as a band gap opening and its transformation into semiconductor.[56–61]

Since the interaction between the graphene or silicene and the substrate can change their electronic properties, these 2D metamaterials acting on a nanoelectronic device need to be placed on insulating substrates. Therefore, the choice of the insulating substrate where the graphene or the silicene is supported could bring benefits to the nanoelectronic device based on graphene or silicene.

The manufacture of a silicene-based electronic device is more difficult than that of a graphene-based electronic device,for the transferred silicene in the air is unstable. Hence, the transfer of the silicene via the transfer technique widely used in graphene cannot be used for silicene. However, recent research has shown a method of transferring this 2D metamaterial to a substrate.[62] First, the silicene was synthesized by epitaxial growth on Ag (111) and a thin layer (5 nm) of alumina (Al_2O_3) was added on the silicene. After this step the silicene together with the Ag (111) were rotated at an angle of 180° and deposited on a layer of SiO_2. In this way, the silicene layer was preserved during its transfer and it was possible to manufacture an FET. To complement the manufacture of this FET, part of the Ag (111) layer was removed, so that the remaining parts of this material serve as contacts (source/drain).

In the same way that has already been detailed for graphene, we focus on more detail of the silicene on h-BN. The cohesion energy between the silicene and the h-BN substrate is approximately 0.07 eV to 0.09 eV per atom of silicon, while between the silicene and the metal surface it is 0.5 eV per atom of silicon.[63]

Considering the fact that the cohesive energy between the silicene layer and the silver surface is very high, there are misgivings that the strong energy interaction between these two surfaces can strongly influence the structure of the energy band on the surface of the silicene. In addition, this strong interaction may be sufficient to cause the Dirac cone related to the silicene on Ag (111) to disappear. On the other hand, the weak Van der Waals interactions between the silicene and the h-BN do not affect the electrical/optical properties of the silicene. Therefore, due to the wide bandgap of h-BN, the silicene should behave as being almost isolated (including the Dirac cone), in superstructures made of silicene on h-BN.[63–65]

The upper part of Fig. 8 shows the graphical representation of the overlaying of the silicene layer on h-BN.

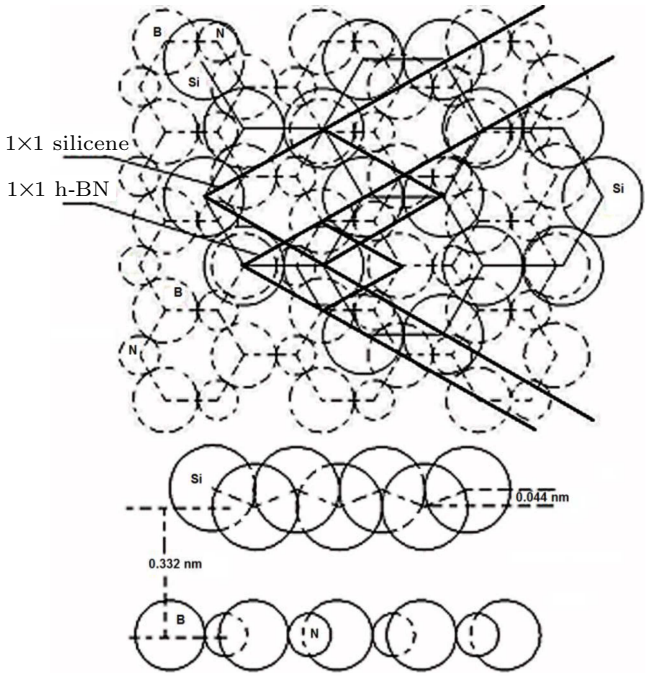


Fig. 8. Top: Atomic structure of silicene on h-BN forming a superstructure. Bottom: Transverse section of the silicene atomic structure on h-BN.

The circles in solid lines represent the atoms of the atomic structure of the silicene, which are positioned on the atomic structure of h-BN, whose circles which are drawn in dash lines represent the atoms of h-BN.

Note that the diamonds represent a unit cell for the silicene and a unit cell for h-BN respectively. The right positioning of the atoms provides the alignment between the atomic structures of the silicene and the h-BN, as we can see in the upper part of Fig. 8.

According to the above-mentioned, while the h-BN atoms are spaced by 0.144 nm and the h-BN structure parameter is 0.25 nm, the minimum distance between the atoms of the silicene is 0.2217 nm and the silicene structure parameter is 0.384 nm.

The interactions between these two atomic structures provide the opening of a band gap at the Dirac points (K) of the silicene, whose value is approximately 30 meV, which does not depend on the rotation between the alignments of the structures of the h-BN and silicene.[64] It is important to state that the bandgap value is caused by the distance between the layers of silicene and h-BN, whose value is 0.332 nm, according to what can be seen in the lower part of Fig. 8.[63,66]

It is noteworthy that the Van der Waals interactions, although weak, are sufficient to join the silicene to the h-BN, forming a superstructure with a Moiré pattern.

The dispersion relation of the silicene on h-BN in the vicinity of the Fermi level can be found by the tight-binding model according to Eq. (6), that is, $E(k) = \pm\sqrt{\Delta^2 + \hbar^2 V_F^2 k^2}$, where Δ is the energy difference between the electrons located in the two superstructures. Consequently, the band gap caused at the K point is given by $E_g = 2\Delta$. Considering the fact that the Van der Waals interaction is weak, the value of Δ is small, which implies a small value for the band gap. It is worth mentioning that the value of this band gap can be increased by changing the interaction between the two substrates, or by applying a gate voltage. Note that the control of the band gap value via gate voltage has already been detailed above.

Besides the h-BN, some other insulating material can act as substrate to support graphene and silicene, preserving its necessary physical characteristics, so that they can constitute future efficient optoelectronic nanodevices. For example, graphene can be obtained from silicon carbide (SiC) via high temperature treatment (HTT), with the advantage that thermal decomposition is a relatively simple process and can be performed over a wide temperature range (1400 K $\sim$ 2000 K), under a high or medium vacuum.[67]

Silicon carbide crystal structure has polytypism, i.e., silicon carbide exists in about 250 crystalline forms.[68] Indeed, the polymorphism of SiC has a large family of similar crystalline structures (polytypes), which can be described by a usual hexagonal axis system, with one c-axis perpendicular to three equivalent axes a, b, and d having angles 120° with one another. All crystallographic modifications have very similar structures, which consist of identical layers perpendicular to the hexagonal or trigonal axes. The (0001) (silicon-terminated) or (000-1) (carbon-terminated) faces of 4H–SiC and 6H–SiC wafers can be used for growing the graphene.[69]

Graphene growth on SiC can be done in a variety of ways, for example, in flat SiC surfaces,[70,71] SiC structured surfaces,[72] and discrete SiC particles.[73] It is noteworthy that after the growing graphene on SiC, the SiC that has been used can serve as a substrate for manufacturing the electronic graphene/SiC devices, thereby avoiding assemblying and/or transferring the graphene films to the SiC used by graphene production methods via mechanical exfoliation, for example.[74,75]

With respect to the silicene, it has been proven that the semi-metallic behavior of silicene embedded in ultra-thin layers of aluminum nitride (AIN), which is considered as an insulating (energy gap about 4.6 eV), can be preserved.[76] In this case, the thin layer of silicene interacts very weakly with the AIN layer through van der Waals (vdW) force.

Partial charge densities in the energy range of $E_F/E_F - 0.2$ eV of silicene on h-BN and of silicene on hydrogenated Si-terminated silicene carbide SiC (0001) surface (Si–SiC) are concentrated on silicene (in the same way as that in free-standing silicene). However, partial charge densities related to silicene on hydrogenated C-terminated silicene carbide SiC (0001) surface (C–SiC) are distributed widely in silicene and substrate, so that in this case, E_F approaches to the maximum value of the C–SiC valence band. Therefore, silicene on hydrogenated Si-terminated silicene carbide SiC (0001) surface (Si–SiC) maintains the Dirac cone, and its geometry and electronic properties are preserved. On the other hand, silicene on hydrogenated C-terminated silicene carbide SiC (0001) surface (C–SiC) has metallic behavior.[77]

Molybdenite, i.e., MoS_2 is a transition metal dichalcogenide (TMD) that classifies as a material of van der Waals. While the band gap of bulk MoS_2 is 1.29 eV, and the band gap of MoS_2 monolayer is 1.90 eV.[78]

Previous studies have shown that the energy conversion energy efficiency of photovoltaic cells based on Schottky diode is significantly increased, when an MoS_2 layer is inserted into the junction region (contacting graphene) between the graphene layer (in the case of trilayer-graphene) and the n-Si layer. The photovoltaic cell constituted by Indium electrode/n-Si substrate/SiO_2 layer/MoS_2 layer ($\approx$ 9 nm)/trilayer-graphene/Au electrode presented an energy conversion efficiency of 11.1%. The correct determination of the thickness of the MoS_2 layer contributes significantly to the increase of the energy conversion efficiency. This is because the MoS_2 layer separates the graphene from the n-Si substrate, which penetrates through a hole in the SiO_2 layer until it encounters the MoS_2 layer. Considering that the MoS_2 layer acts as a charge recombination reducer at the junction, the optical loss decreases, thus increasing the energy conversion efficiency. Another reason that contributes to the increase of the energy conversion efficiency related to this nanophotonics photovoltaic cell is the correct determination of the number of layers of graphene (in this case trilayer-graphene), since this number of graphene layers can reduce the value of the Schottky diode resistance.[79]

On the other hand, previous research has shown that the heterostructure consisting of silicene and MoS_2 occurs, when an Si atom of the unit cell is located directly above an S atom and the another silicon atom is located on the empty part of the MoS_2.[80] In this case, the binding energy is $E_b = 120.32$ meV per atom of silicon, which is sufficient to provide the stability of the silicene.[81] Note that in this case, the distance between two consecutive layers is 0.293 nm, therefore greater than the sum of the covalent rays of Si and S atoms. Hence, the interaction between silicene and MoS_2 layers is a weak vdW-like interaction. Therefore, in this structure, the linear energy bands are preserved and the opening of a band gap occurs (due to the breaking of symmetry caused by the intrinsic interface dipole). The band gap in the silicene/MoS_2 heterostructure is caused by the difference in electron density distribution in this integrated plane.[81]

There are two forms of silicene/MoS_2 heterostructures: high-buckled silicene (HSMS) and low-buckled silicene (LSMS). In both formats, the covalent bonds of the silicene are maintained (without breaking). However the HSMS format presents metallic behavior, unlike what happens in the LSMS format, which is more stable and its band gap can be controlled by gate voltage, in the same way as that in the case of silicene/h-BN.

5. Charge mobilities and charge densities

Previous studies have demonstraded that the isolated graphene has a charge carrier mobility value of 2×10^5 $cm^2{\cdot}V^{-1}{\cdot}s^{-1}$ at room temperature.[82,83] However, more recent studies have shown that the mobility of the isolated graphene is 3.39×10^5 $cm^2{\cdot}V^{-1}{\cdot}s^{-1}$ for electrons and it is 3.22×10^5 $cm^2{\cdot}V^{-1}{\cdot}s^{-1}$ for holes at room temperature.[84] On the other hand, the mobility of graphene over SiO_2 is only 10×10^3 $cm^2{\cdot}V^{-1}{\cdot}s^{-1}$ [85] and the value of the charge mobility of graphene on h-BN is $\mu=2.5\times10^4$ $cm^2{\cdot}V^{-1}{\cdot}s^{-1}$ at high charge densities.[35]

With respect to silicene, recent research has shown that the isolated silicene has an electron mobility of 2.57×10^5 $cm^2{\cdot}V^{-1}{\cdot}s^{-1}$ and a hole molibity of 2.22×10^5 $cm^2{\cdot}V^{-1}{\cdot}s^{-1}$ at room temperature.[85]

In the same way as that in the case of graphene, the mobility of the charge carriers in the silicene depends greatly on the substrate where it is embedded, and the h-BN is one of the substrates which offers a relatively high mobility for the silicene.[45]

The symmetric shapes of the energy dispersion relation in graphene for the conduction and valence bands provide equal group velocity for electrons and holes. In other words, considering ideal graphene (without defects and impurities), or isotropic scattering graphene, that is, when scattering mechanisms affect electrons and holes with the same intensities, the average velocity of the charge due to the presence of an electric field ($V_{\rm drift}$) is the same for electrons and holes. Then, in ideal graphene, the mobility of electrons ($\mu_{\rm e}$) is equal to the mobility of holes ($\mu_{\rm h}$).

The charge mobility can be determined from the measurement of resistivity in a high charge density regime (called metallic regime), where the induced charges do not change the resistivity significantly, according to the following equation:

$$\mu_{\rm e,l}=\frac{1}{en\rho}, \tag{7}$$

where ρ is the electrical resistivity of graphene.

The density of charge carriers for intrinsic graphene is given by $n_0=\sqrt{(n^*/2)^2+n_{\rm th}^2}\approx0.3\times10^{12}$ cm^{-2}, where $n_{\rm th}$ is the contribution due to the generation of charge carriers at the due temperature and n^* is the contribution due to the charges coming from the substrate.

The application of a gate voltage provides an increase in charge density, owing to the fact that graphene (or silicene) and the dielectric substrate form a capacitor (whose capacitance is constituted by the quantum capacitance of the graphene, in series with the capacitance referring to electrode, dielectric and graphene). For the device we are presenting, the quantum capacitance of graphene (or silicene) can be neglected,[86] so that the contribution to the charge density due to the application of gate voltage ($n_{\rm g}$), without taking into account the unbalanced loads due to imperfections, among other factors, is given by

$$n_{\rm g}=\frac{\varepsilon_0\varepsilon V_{\rm g}}{te}, \tag{8}$$

where t is the thickness of the dielectric.

However, taking into account the ambient temperature ($T=300$ K), which causes the value of $K_{\rm B}T\approx26$ meV and the chemical potential of the graphene $\mu_{\rm q}\approx E_{\rm F}\gg K_{\rm B}T$, the application of gate voltage provides a great change in the total charge density in graphene, given by[26]

$$n=\frac{\mu_q^2}{\hbar^2}\cdot\frac{1}{\pi V_{\rm F}^2}, \tag{9}$$

where $\hbar$ is the reduced Planck constant.

For example, considering the Eq. (7) and using $\mu_{\rm q}=0.5$ eV we obtain $n=1.837\times10^{13}$ cm^{-2}.

It is noteworthy that the chemical potential of graphene is given by[87]

$$\mu_{\rm c}=\hbar V_{\rm F}\sqrt{n\pi}. \tag{10}$$

Moreover, the value of the gate voltage ($V_{\rm g}$) is related to the Fermi level (the value is approximately the same as the value of the chemical potential), according to the following equation[88]

$$E_{\rm F}\cong\mu_{\rm q}=\hbar V_{\rm F}\sqrt{\frac{\pi\varepsilon_0\varepsilon_{\rm d}}{ed}(V_{\rm g}-V_{\rm D})}, \tag{11}$$

where $\varepsilon_0\varepsilon_{\rm d}$ is the electrical permittivity of the h-BN and $V_{\rm D}$ is the Dirac voltage (gate voltage value where the maximum resistivity value occurs, i.e., minimum conductivity of the nanoribbon). Note that in an ideal 2D nanoribbon, the gate voltage value at which the maximum resistivity value occurs is $V_{\rm g}=V_{\rm D}=0$. However, in an actual 2D metamaterial nanoribbon there is an intrinsic doping, due to the presence of the unbalanced charge carriers. Therefore, the value of the maximum resistivity of a 2D metamaterial nanoribbon occurs, when $V_{\rm g}=V_{\rm D}$. The use of a dry process of transfer of the graphene to an SiO_2/Si substrate yields $V_{\rm D}<4.5$ V, the average value being around 2.5 V.[89] However, during the investigations of the low frequency flicker noise in a graphene layer on h-BN/SiO_2/Si and on SiO_2/Si, different values of $V_{\rm D}$ for the graphene on h-BN/SiO_2/Si and on SiO_2/Si were found(Please, replace this text: that $V_{\rm D}\approx5$ V for the graphene on substrate h-BN/SiO_2/ Si and $V_{\rm D}\approx2.5$ V for the graphene on the substrate SiO_2/Si).[90] It is worth mentioning that we adopted

$V_D = 4.5$ V. (Please, replace this text: Then, we adopted $V_D = 4.5$ V.)

On the other hand, the concentration of charges in a range of energy (in this case, referring to the device shown in Fig. 5) can be obtained by integrating the Fermi–Dirac distribution function over the energy band. Hence the concentration of charges is given by $n = \int D(E) f_F(E)\,dE$, where $D(E)$ and $f_F = \left(1 + e^{(E-E_f)/(K_B T)}\right)^{-1}$ are the available energy states (density of states (DOS)) and the distribution function of Fermi–Dirac, respectively.

After several mathematical interventions, the total concentration of electrons in the silicene can be determined from[91]

$$n = \frac{2WL}{\pi\hbar^2 V_F^2}\left[\Delta\Gamma(1) K_B T I_0(\eta) + \Gamma(2)(K_B T)^2 I_1(\eta)\right], \quad (12)$$

where W and L are the width and the length of the silicene nanoribbon, respectively, $\eta = (E_F - \Delta)/K_B T$, Γ, K_B, T, and I_i being the gamma function, the Boltzmann constant, the temperature, and the Fermi–Dirac integral, respectively.

Figure 9 shows the charge densities in graphene and in silicene as a function of gate voltage ranging from 5 V to 60 V (E_f ranging from 0.1965 eV to 1.2743 eV) .

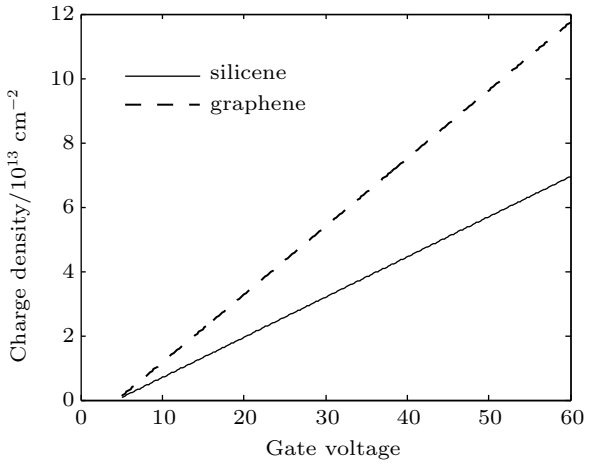


Fig. 9. Charge densities on graphene and silicene as a function of gate voltage.

For high values of V_g (which lead to high values of the chemical potential ($\mu_q \approx E_f$)), $\Delta \ll E_f$. In this case, equation (12) becomes Eq. (9), considering the Fermi velocity for the silicene.

In Fig. 9 it is shown that the charge densities in graphene (Eq. (9)) and in silicene (Eqs. (9) and (12)) as a function of gate voltage (ranging from 5 V to 60 V, which causes E_f to vary from 0.1965 eV to 1.2743 eV).

As we can see from Fig. 9, the charge densities in graphene and in silicene increase linearly with the increase in the gate voltage, but in graphene the charge density is slightly higher than in silicene due to the fact that the Fermi velocity in graphene is slightly higher than in silicene.

6. Conductivities and absorptions

Graphene and silicene in their original states (without doping) have Fermi energy $E_F = 0$ at the K points of the Brillouin zone (Dirac points), where the valence band is completely filled while the conduction band is completely empty. The conduction and valence bands touch the K points, andnear these points the dispersion relation can be considered to be linear. In this case, the optical excitations cause electron-hole excitations, called intraband and interband transition, according to what is shown in Fig. 10.

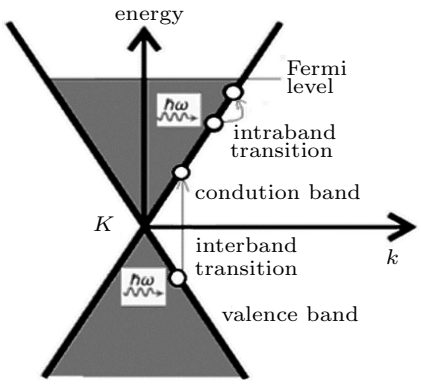


Fig. 10. Schematic representation of intraband and interband transitions.

Hence, the optical conductivities of graphene and silicene are determined by intraband and interband transitions, which can be obtained from the Drude model,[92] given by[93–95]

$$\sigma(w) = \sigma_{DC}(E_F)/(1 + w^2\tau^2), \quad (13)$$

where σ_{DC} is the direct current (DC) conductivity and w is the angular frequency of the incident photon, and τ is the relaxation time (period of time in which an electron can move freely after its previous collision).

Actually, the conductivities of graphene and silicene are the sum of the contributions referring to the intraband and interband excitations, which can be calculated using the Kubo formula. Considering that we are dealing with angular frequencies $w \gg 1/\tau$, i.e., $\beta_F < w \to n_{eff} < c/V_F \approx 300$, where n_{eff} is the effective refractive index ($n_{eff} = \beta/_0$; $k_0 = 2\pi\lambda_0$), β is the wave number for the GSPP mode, λ_0 is the wavelength of the photon in free space and c is the speed of light in the vacuum; under these conditions the intraband conductivity of graphene is given by[87,96,97]

$$\sigma_{intra}(w,\mu_c) = \frac{i e^2 \mu_c}{(\omega + i\tau^{-1})\pi\hbar^2}, \quad (14)$$

where the relaxation time (τ) is given by[26,98]

$$\tau = \frac{\mu_c \mu}{e V_F^2} \quad (15)$$

and the interband conductivity of graphene is given by[87,96]

$$\sigma_{inter} = \frac{e^2}{4\hbar}\left[1 + \frac{i}{\pi}\ln\frac{\hbar(\omega + i\tau^{-1}) - 2\mu_c}{\hbar(\omega + i\tau^{-1}) + 2\mu_c}\right]. \quad (16)$$

For high frequencies ($w \gg \mu_c, K_B T$), the conductivity of graphene is given by $\sigma_0 = e^2/(4\hbar) \approx 6.08 \times 10^{-5}\ \Omega^{-1} =>$ 0,[87] σ_0 being defined as the universal conductivity of graphene, which can also be represented by $\sigma_0 = \pi_0/4$, where $G_0 = 2e^2/h$ is what is called quantum of conductance.[99]

In Fig. 11 we show the graphs of the real (left part) and imaginary (right part) referring to the intraband, interband, and total, of the graphene embedded in h-BN, as a function of $0 \leq \mu_c \leq 1$ (eV), for $\lambda = 1.5317024$ μm, which belongs to the *C* band of Telecommunication Standardization Sector - ITU (on the top of Fig. 11) and for frequency $f = 10$ THz (on the bottom of Fig. 11).

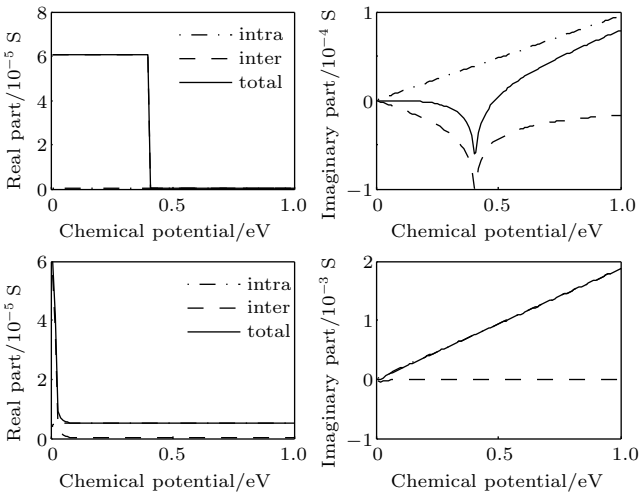


Fig. 11. Upper: Conductivity of graphene embedded in h-BN for $\lambda = 1.5317024$ μm. Bottom: Conductivity of graphene embedded in h-BN for $f = 10$ THz.

Note that for $\lambda = 1.5317024$ μm, the total real part of the graphene conductivity (solid line) is provided by the real part of the interband conductivity (dash line), while for $f = 10$ THz ($\lambda = 30$ μm), the total real part of the graphene conductivity is provided by the real part of the intraband conductivity (dash and dotted line). In addition, for $\lambda = 1.5317024$ μm, the total imaginary part of the graphene conductivity (solid line) is obtained by the sum of the imaginary parts of the intraband (dash and dotted line) and interband (dash line) of the graphene conductivity. In this case, the total imaginary part of the graphene conductivity can be negative or positive. On the other hand, for $f = 10$ THz, the total imaginary part of the graphene conductivity is provided by the imaginary part of the intraband contribution. In this case, the total imaginary part of the graphene conductivity is positive. It is worth mentioning that for a positive value of the imaginary part of the conductivity, graphene (and silicene) can support TM modes. (Considering the fact that *x* is in the direction of propagation, TM modes have electromagnetic fields components H_y, E_x, and E_z). We will return to this subject in the next section.

In Fig. 12 are shown the graphs of the real and imaginary parts of the graphene conductivity embedded in h-BN, as a function of wavelength ranging from $\lambda = 1.55$ μm to $\lambda = 30$ μm, for $\mu_c = 0.6$ eV.

As we can see, the imaginary part of the conductivity of graphene is positive over the entire wavelength range.

It is important to state that the universal conductivity shown for graphene is also valid for the chemical elements Si, Ge, and Sn of group IV of the periodic table, constituting a plane (or semiplane) with honeycomb atomic structure.

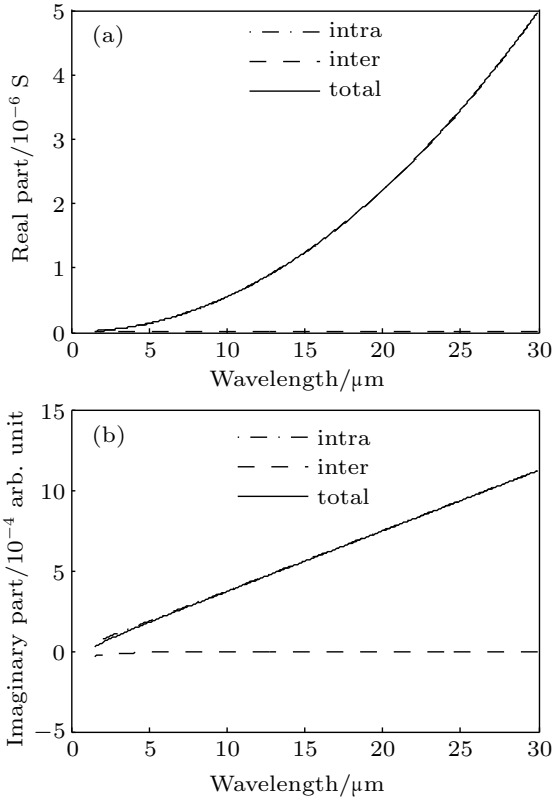


Fig. 12. Real and imaginary parts of the conductivity of graphene embedded in h-BN versus wavelength ($\mu_c = 0.6$ eV).

The complex conductivities of graphene and silicene can also be obtained from their complex permittivities. The real part of the silicene conductivity, for example, can be found through the Ehrenreich–Cohen formula, and the imaginary part of that conductivity from the equation of the real part, via Kramers–Kronig relations concerning the dielectric functions.[100,101] However, by applying the correct values with respect to the physical properties of the silicene, for wavelengths between the THz and infrared frequency region, we can use Eqs. (14)–(16) for determining the real and imaginary parts of the silicene .

It is observed in Eqs. (14) and (16) that in the range of wavelengths from THz to infrared the conductivities of graphene and silicene depend only on the chemical potential and on the relaxation time, which in turn depends only on the values of the chemical potential, Fermi velocity and charge mobility. Therefore, for each wavelength at a fixed chemical potential, as the values of the Fermi velocity and charge mobility for graphene and for silicene are very close to their counterparts, the values for the relaxation times related to those two 2D metamaterials are also very close to each other (for that range of wavelengths), so that the values of the real part and

imaginary part of the conductivity of the graphene and silicene are practically the same.

For a layer of graphene (or silicene) under the normal incidence of electromagnetic waves, the absorption at $\omega > 2\mu_c/\hbar$ is given by $A = \pi\alpha_s/(1+\pi\alpha_s)^2 \approx \pi\alpha_s \approx 2,293\%$, where $\alpha_s = e^2/(4\pi\varepsilon_0\hbar c)$ is the Sommerfeld finestructure constant.[100] This means that universal absorption occurs when $\lambda < \pi c\hbar/\mu_c$. On the top of Fig. 13 are shown the regions of the wavelengths where universal and non-universal absorption occur, as a function of the chemical potential.

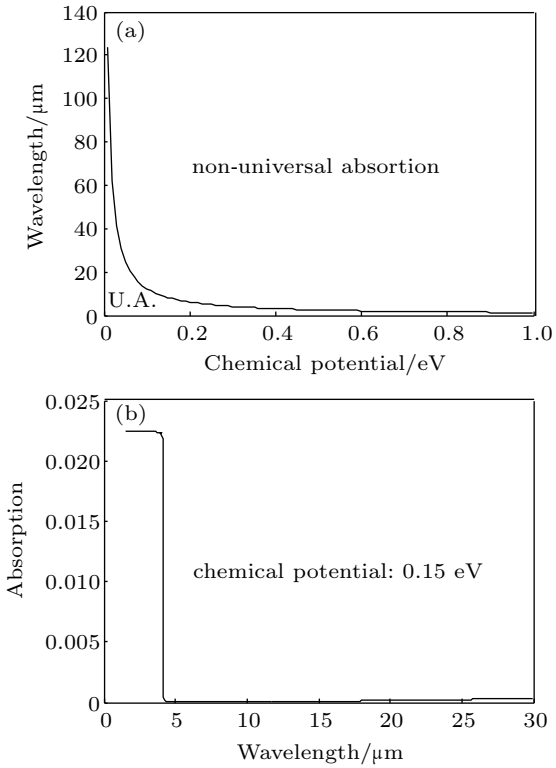


Fig. 13. (a) Range of lengths where universal and non-universal absorption occurs depending on the chemical potential. (b) Absorption as a function of wavelength for $\mu_c = 0.15$ eV.

The following equation can be used to determine the absorption values, with considering normal incidence and the graphene layer (or silicene) embedded in a single dielectric:[101]

$$A = \frac{\mathrm{Re}(\tilde{\sigma}(\omega))}{\left|1+\dfrac{\tilde{\sigma}(\omega)}{2}\right|^2}, \tag{17}$$

where $\tilde{\sigma}(\omega) = \sigma(\omega)/(\varepsilon_0 c)$.

Equation (17) shows the values of the absorption as a function of the wavelength (for $\mu_c = 0.15$ eV) in the lower part of Fig. 13. Note that for $\lambda <\approx 4.133$ μm occurs the value of the universal absorption.

The physical explanation for what was detailed above is that absorptions occur in graphene, when an electron in the valence band absorbs a photon and is excited to an empty state in the conduction band, with the same momentum (interband transitions). However, the interband transition can only occurs when there is a occupied state with Dirac energy $\varepsilon = (-\hbar\omega)/2$ and an empty state with Dirac energy $\varepsilon = (+\hbar\omega)/2$. This means that the interband transition can only occurs, for $\mu_g < \hbar\omega/2$ ("Pauli blocking mechanism"). On the other hand, the intraband transition can also lead to absorption process. This type of transition occurs due to interactions with phonons, but it only exists in a significant amount from the far infrared frequencies until the THz frequencies in the presence of high concentration of charge carriers. Hence, the probability of occurrence of intraband transitions tends to zero, when when $\mu_g \to 0$.

The absorption also depends on the angle of incidence and on the angle of refraction according to the following equation (for TM modes):[100]

$$A = \frac{4\sqrt{\varepsilon}_1 \cos(\theta_1)\,\mathrm{Re}(\tilde{\sigma})}{\left(\sqrt{\varepsilon}_1\cos(\theta_1)+\sqrt{\varepsilon}_2\cos(\theta_2)\right)^2}, \tag{18}$$

where θ_1 and θ_2 are the incidence and refraction angles, respectively, and ε_1 and ε_2 are the dielectric constants of the two media in which the 2D metamaterial is embedded. Figure 14 shows the absorption values (considering $\varepsilon_1 = \varepsilon_2 = 1$) as a function of the incidence angle (ranging from 0 to $\pi/2$ rad), referring to the incidence of violet light ($\lambda = 0.3$ nm, photon energy $E_{ph} \approx 3.1$ eV).

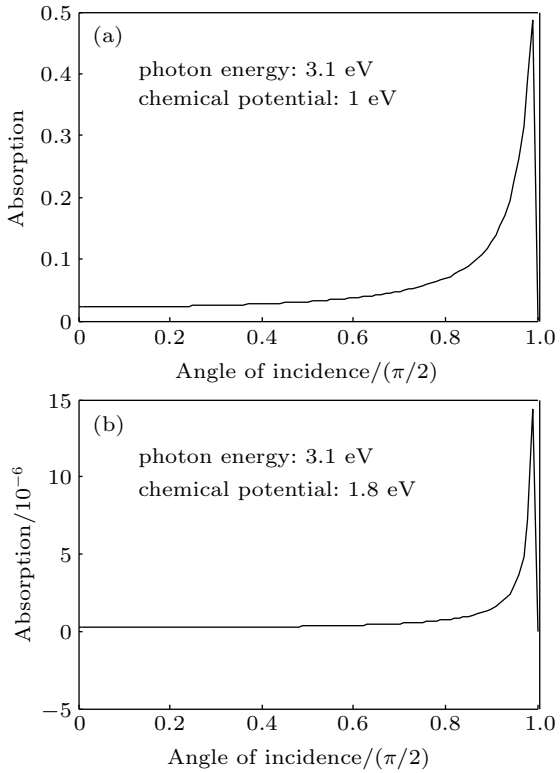


Fig. 14. Absorption versus angle of incidence. (a) $\mu_c = 1$ eV. (b) $\mu_c = 1.8$ eV.

Note that on the top of Fig. 14 is the plot of absorption versus angle of incidence for gate voltage with value $\mu_c = 1$ eV ($< E_{ph}/2$). We can see that for values close to the angle $\pi/2$ rad the absorption increases to approximately 0.5. On the other hand, in the lower part of Fig. 14 is the plot of absorption versus angle of incidence for gate voltage with value $\mu_c = 1.8$ eV ($> E_{ph}/2$). Note that in this case, the absorption is practically null. This occurs due to the fact that $\mu_c > E_{ph}/2$.

We will come back to this subject in the next section. It is noteworthy that although we have shown the absorption as a function of angle of incidence and gate voltage values (for photons in the region of violet light), the above detailed is valid for the entire frequency range, from the THz region to the ultraviolet region.

7. Electrical permitivities, wave vector dispersion relations, TM and TE modes

The electrical permittivity and dielectric constant for an isolated 2D metamaterial can be obtained from the Maxwell equations given by[102]

$$\varepsilon = \varepsilon_0 + \mathrm{i}\frac{\sigma}{\omega t}; \quad \varepsilon_\mathrm{r} = 1 + \mathrm{i}\frac{\sigma}{\omega\varepsilon_0 t}, \tag{19}$$

respectively.

It is obvious that in this case, the refractive index $n = \varepsilon_\mathrm{r})^{0.5}$ is given by

$$n = \sqrt{1 + \mathrm{i}\frac{\sigma}{\omega\varepsilon_0 t}}. \tag{20}$$

Complex refractive index of 2D metamaterial embedded in the same dielectric can be determined as $n = n(\omega) - \mathrm{i}k\omega$, where k is called the extinction coefficient.

We can determine the behavior of the electromagnetic wave in 2D metamaterial, by using the Dyadic Green function and Maxwell's equations and by manipulating the polarization state.[102–104]

Graphene can support TE (polarization p) or TM (polarization s) modes, provided that the imaginary part of its conductivity is negative or positive, respectively (silicene behaves in a similar way to graphene according to what was previously detailed).

From Eq. (14), we can show that the real part of the intraband contribution is null (Figs. 11 and 12), so that only the interband contribution of the conductivity constitutes the real part value of the conductivity of the graphene (and silicene). Note that for values $\hbar\omega/\mu_\mathrm{c} > 2$, the real part of the conductivity of the graphene (σ) is positive according to what can be seen in Fig. 15.

The equation that determines the electrical permittivity in 2D metamaterial already presented above is given by $\varepsilon = \varepsilon_0 + \mathrm{i}(\sigma/(\omega t))$. It is important to state that considering the real and imaginary parts of the conductivity ($\sigma = \sigma' + \sigma''$), this equation can become (from the Maxwell equations) $\varepsilon = \varepsilon_0 - \sigma''/(\omega t) + \mathrm{i}(\sigma'/(\omega t))$. Note that in this case, the real part of the permittivity for each of graphene and silicene is given by $\varepsilon' = \varepsilon_0 - \sigma''/(\omega t)$ and the imaginary part is given by $\varepsilon'' = \mathrm{i}(\sigma'/(\omega t))$. Therefore, the real parts of the permittivity of graphene and silicene can be positive, or negative, depending on the imaginary part of the conductivity of that 2D material. It is worth noting that when the real part of this permittivity is negative, TM modes can exist. On the other hand, when the real part of this permittivity is positive, TE modes can exist. Therefore, in graphene and in silicene, modes TM ($\varepsilon' = \varepsilon_0 + \sigma''/(\omega t) < 0$; $\sigma'' > 0$) or weak TE modes ($\varepsilon' = \varepsilon_0 + \sigma''/(\omega t) > 0$; $\sigma'' < 0$) can occur,[105] according to what can be seen in Fig. 15. Hence, SPP modes TM and TE are supported in graphene, for $0 < \hbar\omega/\mu_\mathrm{g} < 1.667$ and $1.667 < \hbar\omega/\mu_\mathrm{g} < 2$, respectively.[106,107]

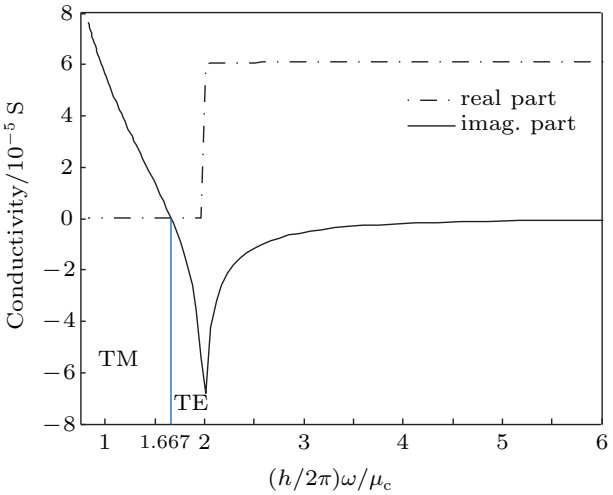


Fig. 15. (color online) Graphene conductivity as a function of $\hbar\omega/\mu_\mathrm{c}$.

Moreover, the increase in temperature causes the real parts of the conductivity of graphene and silicene at the point of bifurcation to slightly change (where $\sigma' = 0$), so that the real part of the conductivity becomes slightly positive for some values of $\hbar\omega/\mu_\mathrm{g} \approx < 2$. Hence, in this case small attenuations occur in the SPP modes, and TE modes suffer greater attenuations.[105]

The dispersion relation for the TM mode on a sheet of graphene embedded in a dielectric can be obtained from Maxwell's equations, given by[108]

$$\sqrt{q^2 - \frac{\omega^2\varepsilon_\mathrm{d}}{c^2}} = -\frac{2\omega\varepsilon_0\varepsilon_\mathrm{d}}{\mathrm{i}\sigma}, \tag{21}$$

where q is the wave number of the GSPP modes, $\omega = ck_0$ and ε_d is the dielectric constant of the medium in which graphene or silicene is embedded.

From Eq. (21), we can obtain the following dispersion relation for TM modes:[98]

$$q_\mathrm{TM}^2 = k_0^2\left[\varepsilon_\mathrm{d} - \left(\frac{2\varepsilon_\mathrm{d}}{\eta_0\sigma_\mathrm{g}}\right)^2\right], \tag{22}$$

where ε_d is the relative permittivity of the dielectric, η_0 is the air impedance and $\eta_0 = 377\ \Omega$, and $k_0 = 2\pi\lambda_0$.

On the other hand, the dispersion relation for GSPPs TE mode on a graphene (or silicene) surface can be determined according to the following equation:[107]

$$q_\mathrm{TE}^2 = k_0^2\left[\varepsilon_\mathrm{d} - \left(\frac{\eta_0\sigma_\mathrm{g}}{2\varepsilon_\mathrm{d}}\right)^2\right]. \tag{23}$$

The wavelength for a GSPP mode propagating through a graphene or silicene nanoribbon, and its propagation distance, i.e., the distance that this mode can propagate until its intensity decreases to $1/e$ of its value, are given by[109–112]

$$\lambda_{\mathrm{GSPP}} = \frac{2\pi}{\mathrm{Re}\,[q]};\ L_{p_{\mathrm{GSPP}}} = \frac{1}{2\,\mathrm{Im}\,[q]}. \tag{24}$$

8. Conclusions

The 2D metamaterial (in which atoms constitute a plane or a semi-plane) is considered to be of great relevance to the progress in all exact sciences. Since the discovery of graphene, researchers around the world have increasingly investigated in depth the details of the electrical/optical properties relating to the other two-dimensional (2D) metamaterials, such as silicene. The huge interest in silicene occurs due to the usage of silicon in the optoelectronic industry. Note that the constant advance in the technology related to the silicene allows us to inform that it will most probably be possible to find the solution to enable Moore's law in dimensions smaller than 10 nm.

In this review, we include the details and comparisons of the atomic structures, diagrams of energy bands, substrates, charge densities, charge mobilities, conductivities, absorptions, electrical permittivities, dispersion relations of the wave vectors and supported electromagnetic modes referring to the graphene and to the silicene. Hence, we have developed the subjects most relevant to the professional life of those who work in the area of nanotechnoly and nanophotonics based in graphene or silicene.

References

[1] Ozawa E, Kroto H W, Fowler P W and Wassermann E 1993 *Phil. Trans. R. Soc. A* **343** 1
[2] Takeda K and Shiraishi K, 1994 *Phys. Rev. B* **50** 14916
[3] Lalmi B, Oughaddou H, Enriquez H, Kara A, Vizzini S, Ealet B and Aufray B 2010 *Appl. Phys. Lett.* **97** 223109
[4] Aufray B, Kara A, Vizzini S, Oughaddou H, Leandri C, Ealet B and Le Lay G 2010 *Appl. Phys. Lett.* **96** 183102
[5] Liu C, Feng W and Yao Y 2011 *Phys. Rev. Lett.* **107** 076802
[6] Takeda K and Shiraishi K 1994 *Phys. Rev. B* **50** 14916
[7] Durgun E, Tongay S and Ciraci S 2005 *Phys. Rev. B* **72** 075420
[8] Cahangirov S, Topsakal M, Aktürk E, Ahin H S and Ciraci S 2009 *Phys. Rev. Lett.* **102** 236804
[9] Vogt P, De Padova P, Quaresima C, Avila J, Frantzeskakis E, Asensio M C, Resta A, Ealet B and Le Lay G 2012 *Phys. Rev. Lett.* **108** 155501
[10] Jamgotchian H, Colignon Y, Hamzaoui N, Ealet B, Hoarau J, Aufray B and Bibérian J 2012 *J. Phys.: Condens. Matter* **24** 172001
[11] Feng B, Ding Z, Meng S, Yao Y, He X, Cheng P, Chen L and Wu K 2012 *Nano Lett.* **12** 3507
[12] Enriquez H, Vizzini S, Kara A, Lalmi B and Oughaddou H 2012 *J. Phys.: Condens. Matter* **24** 314211
[13] Chen L, Liu, C C, Feng B, He X, Cheng P, Ding Z, Meng S, Yao Y and Wu K 2012 *Phys. Rev. Lett.* **109** 056804
[14] Lin C L, Arafune R, Kawahara K, Tsukahara N, Minamitani E, Kim Y, Takagi N and Kawai M 2012 *Appl. Phys. Express* **5** 045802
[15] Fleurence A, Friedlein R, Ozaki T, Kawai H, Wang Y and Yamada-Takamura Y 2012 *Phys. Rev. Lett.* **108** 245501
[16] Durajski A, Szczes'niak D and Szczes'niak R 2014 *Solid State Commun.* **200** 17
[17] Chen L, Feng B and Wu K 2013 arXiv: 1301.1431
[18] Guzmán-Verri G G and Lew Yan Voon L C 2007 *Phys. Rev. B* **76** 075131
[19] Lew Yan Voon L C, Zhu J and Schwingenschlögl U 2016 *Appl. Phys. Rev.* **3** 040802
[20] Suzuki T and Yokomizo Y 2010 *Physica E: Low-Dimensional Systems and Nanostructures* **42** 2820
[21] Houssa M, Pourtois G, Afanas'ev V V and Stesmans A 2010 *Appl. Phys. Lett.* **97** 112106
[22] Kara A, Enriquez H, Seitsonen A P, Lew Yan Voon L C, S, Vizzini, Aufray B and Oughaddou H 2012 *Surf. Sci. Rep.* **67** 1
[23] Lebegue S and Eriksson O 2009 *Phys. Rev. B* **79** 115409
[24] Liu C C, Jiang H and Yao Y 2011 *Phys. Rev. B* **84** 195430
[25] Zhang L, Fu X L, Lei M, Chen J J, Yang J Z, Peng Z J and Tang W H 2014 *Chin. Phys. B* **23** 038101
[26] Christensen J, Manjavacas A, Thongrattanasiri S, Koppens F H L and Abajo F J G 2012 *ACS Nano* **6** 431
[27] Nikitin A Y, Guinea F, García-Vidal F J and Martín-Moreno L 2011 *Phys. Rev. B* **84** 161407(R)
[28] Wirth-Lima A J, Moura J C N and Sombra A S B 2015 *Beilstein J. Nanotechnol.* **6** 1221
[29] Young A F, Dean C R, Meric I, Sorgenfrei S, Ren H, Watanabe K, Taniguchi T, Hone J K, Shepard L and Kim P 2010 "Electronic compressibility of gapped bilayer graphene", arXiv: 1004.5556v2
[30] Murali R, Yang Y, Brenner K, Beck T and Meindl J D 2009 *Appl. Phys. Lett.* **94** 243114
[31] Wang H, Taychatanapat T, Hsu A, Watanabe K, Taniguchi T, Jarillo-Herrero P and Palacios T 2011 *IEEE Electron Dev. Lett.* **32** 1209
[32] Taniguchi T and Watanabe K 2007 *J. Crystal Growth* **303** 525
[33] Watanabe K, Taniguchi T and Kanda H 2004 *Nat. Mater.* **3** 404
[34] Nanotubes and Nanosheets 2005 Taylor e Francis group (CRC Press) ISBN: 13:978-1-4665-9810-2
[35] Dean C R , Young A F , Meric I, Lee C, Wang L, *et al.*, 2010 *Nat. Nanotechnol.* **5** 722
[36] Léandri C, Oughaddou H, Aufray B, Gay J M, Le Lay G, Ranguis A and Garreau Y 2007 *Surf. Sci.* **601** 262
[37] De Padova P, Quaresima C, Olivieri B, Perfetti P and Le Lay G 2011 *J. Phys. D: Appl. Phys.* **44** 312001
[38] Feng B, Ding Z, Meng S, Yao Y, He X, Cheng P, Chen L and Wu K 2012 *Nano Lett.* **12** 3507
[39] Lin C L, Arafune R, Kawahara K, Tsukahara N, Minamitani E, Kim Y, Takagi N and Kawai M 2012 *Appl. Phys. Express* **5** 045802
[40] Jamgotchian H, Colignon Y, Hamzaoui N, Ealet B, Hoarau J Y, Aufray B and Biberian J P 2012 *J. Phys.: Condens. Matter* **24** 172001
[41] Chen L, Liu C C, Feng B, He X, Cheng P, Ding Z, Meng S, Yao Y and Wu K 2012 *Phys. Rev. Lett.* **109** 056804
[42] Feng B, Ding Z, Meng S, Yao Y, He X, Cheng P, Chen L and Wu K 2012 *Nano Lett.* **12** 3507
[43] Gao J and Zhao J 2012 *Sci. Rep.* **2** 861
[44] Guo Z X, Furuya S, Iwata J I and Oshiyama A 2013 *Phys. Rev. B* **87** 235435
[45] Zhao J *et al.*, 2016 *Prog. Mater. Sci.* **83** 24
[46] Liu Z L, Wang M X, Xu J P, Ge J F, Lay G L, Vogt P, *et al.*, 2014 *New J. Phys.* **16** 075006
[47] Feng B, Ding Z, Meng S, Yao Y, He X, Cheng P, *et al.*, 2012 *Nano Lett.* **12** 3507
[48] Meng L, Wang Y, Zhang L, Du S, Wu R, Li L, Zhang Y, Li G, Zhou H, Hofer W A and Gao H J 2013 *Nano Lett.* **13** 685
[49] Chiappe D, Scalise E, Cinquanta E, Grazianetti C, van den Broek B, Fanciulli M, Houssa M and Molle A 2014 *Adv. Mater.* **26** 2096
[50] Chen H, Chien K, Lin C, Chiang T and Lin D 2016 *J. Phys. Chem. C* **120** 2698
[51] De Padova P, Vogt P, Resta A, Avila J, Razado-Colambo I, Quaresima C, Ottaviani C, Olivieri B, Bruhn T, Hirahara T, Shirai T, Hasegawa S, Carmen Asensio M and Le Lay G 2013 *Appl. Phys. Lett.* **102** 163106
[52] De Padova P, Avila J, Resta A, Razado-Colambo I, Quaresima C, Ottaviani C, Olivieri B, Bruhn T, Vogt P, Asensio M C and Le Lay G 2013 *J. Phys.: Condens. Matter* **25** 382202
[53] Vogt P, Capiod P, Berthe M, Resta A, De Padova P, Bruhn T, Le Lay G and Grandidier B 2014 *Appl. Phys. Lett.* **104** 021602
[54] Salomon E, El Ajjouri R, Le Lay G and Angot T 2014 *J. Phys.: Condens. Matter* **26** 185003
[55] De Padova P, Ottaviani C, Quaresima C, Olivieri B, Imperatori P, Salomon E, Angot T, Quagliano L, Romano C, Vona A, Muniz-Miranda M, Generosi A, Paci B and Le Lay G 2014 *2D Materials* **1** 021003

[56] Houssa M, Pourtois G, Afanas'ev V V and Stesmans A 2010 *Appl. Phys. Lett.* **97** 112106

[57] Lew Yan Voon L C, Sandberg E, Aga R S and Farajian A A 2010 *Appl. Phys. Lett.* **97** 163114

[58] Houssa M, Scalise E, Sankaran K, Pourtois G, Afanas'ev V V and Stesmans A 2011 *Appl. Phys. Lett.* **98** 223107

[59] Wang X Q, Li H D and Wang J T 2012 *Phys. Chem. Chem. Phys.* **14** 303

[60] Zhang C W and Yan S S 2012 *J. Phys. Chem. C* **116** 4163

[61] Osborn T H, Farajian A A, Pupysheva O V, Aga R S and Lew Yan Voon L C 2011 *Chem. Phys. Lett.* **511** 101

[62] Tao L, Cinquanta E, Chiappe D, Grazianetti C, Fanciulli M, Dubey M, Molle A and Akinwande D 2015 *Nat. Nanotechnol.* **10** 227

[63] Kaloni T P, Tahir M and Schwingenschlogl U 2013 *Sci. Rep-Uk.* **3** 3192

[64] Liu H S, Gao J F and Zhao J J 2013 *J. Phys. Chem. C* **117** 10353

[65] Li L Y, Wang X P, Zhao X Y and Zhao M W 2013 *Phys. Lett. A* **377** 2628

[66] Kim J H and Lee Z 2014 *Applied Microscopy*, pISSN 2287-5123, eISSN 2287-4445

[67] Emtsev K V, Bostwick A, Horn K, Jobst J, Kellogg G L, Ley L, McChesney J L, Ohta T, Reshanov S A, Rohrl J, *et al.*, 2009 *Nat. Mater.* **8** 203

[68] Cheung R 2006 *Silicon carbide microelectromechanical systems for harsh environments*, (Imperial College Press) p. 3, ISBN 1-86094-624-0

[69] Yu X Z, Hwang C G, Jozwiak C M, Köhl A, Schmid A K and Lanzara A 2011 *Journal of Electron Spectroscopy and Related Phenomena* **184** 100

[70] Dharmaraj P, Jeganathan K, Parthiban S, Kwon, J Y, Gautam S, Chae K H and Asokan K 2014 *Appl. Phys. Lett.* **105** 181601

[71] Cavaliere V, Schopfer F, Mailly D, Poirier W and Ouerghi A 2014 *Sci. Rep.* **4** 4558

[72] Hu Y, Ruan M, Guo Z, Dong R, Palmer J, Hankinson J, Berger C and Heer W A D 2012 *J. Phys. D: Appl. Phys.* **45** 154010

[73] Zhu K, Guo L, Lin J, Hao W, Shang J, Jia Y, Chen L, Jin S, Wang W and Chen X 2012 *Appl. Phys. Lett.* **100** 023113

[74] Novoselov K S, Geim A K, Morozov S V, Jiang D, Zhang Y, Dubonos S V, Grigorieva I V and Firsov A A 2004 *Science* **306** 666

[75] Yi M and Shen Z 2015 *J. Mater. Chem. A* **3** 11700

[76] Houssa M, Pourtois G, Afanas'ev V V and Stesmans A 2010 *Appl. Phys. Lett.* **97** 112106

[77] Liu H, Gao J and J Zhao 2014 *Journal of Physics: Conference Series* **491** 012007

[78] Mak K F, Lee C, Hone J, Shan J and Heinz T F 2010 *Phys. Rev. Lett.* **105** 136805

[79] Tsuboi Y, Wang F, Kozawa D, Funahashi K, Mouri S, Miyauchi Y, Takenobu T and Matsuda K 2015 *Nanoscale* **7** 14476

[80] Li X D, Wu S Q, Zhou S and Zhu Z Z 2014 *Nanoscale Res. Lett.* **9** 110

[81] Gao N, Li J C and Jiang Q 2014 *Phys. Chem. Chem. Phys.* **16** 11673

[82] Chen J H, Jang C, Xiao S D, Ishigami M and Fuhrer M S 2008 *Nat. Nanotechnol.* **3** 206

[83] Morozov SV, Novoselov K S, Katsnelson M I, Schedin F, Elias D C, Jaszczak J A and Geim A K 2008 *Phys. Rev. Lett.* **100** 016602

[84] Shao Z G, Ye X S, Yang L and Wang C L 2013 *J. Appl. Phys.* **114** 093712

[85] Nagashioa K, Yamashita T, Nishimura T, Kita K and Toriumi A 2011 *J. Appl. Phys.* **110** 024513

[86] Fisichella G, Di Franco S, Fiorenza P, *et al.*, 2013 *Beilstein J. Nanotechnol.* **4** 234

[87] Gan C H, Chu H S and Li E P 2012 *Phys. Rev. B* **85** 125431

[88] Xu F, Das S, Gong Y, Liu Q, Chien H C, Chiu H Y, Wu J and Hui R 2015 *Appl. Phys. Lett.* **106** 031109

[89] Abhilash T S, De Alba R, Zhelev N, Craigheadb H G and Parpia J M 2015 *Nanoscale* **7** 14109

[90] Kayyalha M and Chen Y P 2015 *Appl. Phys. Lett.* **107** 113101

[91] Sadeghi H 2014 *J. Nanosci. Nanotechnol.* **14** 4178

[92] Sensale-Rodriguez B, Yan R, Kelly M, Fang T, Tahy K, Hwang W S, Jena D, Liu L and Xing H G 2012 *Nat. Commun.* **3** 780

[93] Dawlaty J, *et al.*, 2008 *Appl. Phys. Lett.* **93** 131905

[94] Choi H, *et al.*, 2009 *Appl. Phys. Lett.* **94** 172102

[95] Winnerl S, *et al.*, 2011 *Phys. Rev. Lett.* **107** 237401

[96] Falkovsky L A and Pershoguba S S 2007 *Phys. Rev. B* **76** 153410

[97] Gusynin V P, Sharapov S G and Carbotte J P 2007 *Phys. Rev. B* **75** 165407

[98] Wang B, Zhang X, Yuan X and Teng J 2012 *Appl. Phys. Lett.* **100** 131111

[99] Kuzmenko A B, Heumen E, Carbone F and Marel D, 2008 *Phys. Rev. Lett.* **100** 117401

[100] Zhan T, Shi X, Dai Y, Liu X and Zi J 2013 *J. Phys.: Condens. Matter* **25** 215301

[101] Matthes L, Pulci O and Bechstedt F 2014 *New J. Phys.* **16** 105007

[102] Hanson G W 2008 *J. Appl. Phys.* **103** 064302

[103] Pan X Y, Han S and Wang G 2014 *AIP Adv.* **4** 097129

[104] Nikitin A Y, Garcia-Vidal F J and Martin-Moreno L 2013 *IEEE J. Quantum Electron.* **19** 4600611

[105] Vakil A and Engheta N 2011 "One-Atom-Thick IR Metamaterials and Transformation Optics Using Graphene", Cornell University Library, arXiv: 1101.3585v1.

[106] Mikhailov S A and Ziegler K 2007 *Phys. Rev. Lett.* **99** 016803

[107] Luo X, Qiu T, Lu W and Ni Z 2013 "Plasmons in graphene: Recent progress and applications", Elsevier - Materials Science and Engineering: R: Reports, Vol. 74, Issue 11, pp. 351–376

[108] Jablan M, Buljan H and SoljčćM 2009 *Phys. Rev. B* **80** 245435

[109] Barnes W L 2006 *J. Opt. A: Pure Appl. Opt.* **8** S87

[110] Murray W A and Barnes W L 2007 *Adv. Mater.* **19** 3771

[111] Koppens F H L, Chang D E and García de Abajo F J 2011 *Nano Lett.* **11** 3370

[112] Bao Q and Loh K P 2012 *ACS Nano* **6** 3677